IEEE Open Journal of
Industry Applications

Received 19 August 2020; revised 10 October 2020; accepted 13 October 2020. Date of publication 16 October 2020; date of current version 30 October 2020. The review of this article was arranged by Editor F. Briz.

Digital Object Identifier 10.1109/OJIA.2020.3031768

Comparative Analysis of Experimental DC Arc Flash Results to Industry Estimation Methods

COREY S. WEIMANN (Member, IEEE), ROBERT J. KERESTES (Member, IEEE), AND BRANDON M. GRAINGER (Senior Member, IEEE)

Electrical and Computer Engineering Department, University of Pittsburgh, Pittsburgh, PA 15260 USA

CORRESPONDING AUTHOR: BRANDON M. GRAINGER (e-mail: bmg10@pitt.edu)

This work was supported in part by U.S. Department of Energy Award DE-EE0006340 and Award DE-EE0007327, and in part by Mersen Electrical Power, Eaton Corporation, and Wabtec Corporation.

ABSTRACT With the utilization of DC systems increasing, and constant emphasis for worker safety as a top priority for all companies, arc flash feasibility for DC systems is a growing concern. This article details the feasibility of DC arc flash events with experimental scouting tests for a 130 VDC system. Sensitivity studies are experimentally performed on the impact of bus gap distance and bolted fault current level on incident energy. Test results are analyzed and conclusions drawn on the results, in particular incident energies. Details of the tests performed including the setup, procedure, and system parameters are also provided. Theoretical methods of determining incident energy for the testing conditions are also explored. Specifically, these are Doan's and NFPA 70E's maximum power models, and Stokes and Oppenlander's and Paukert's arc resistance models. A comparative analysis of the test results to industry standard, NFPA 70E, and software analysis methods using ETAP, an industry leading software used for arc flash studies, is performed.

INDEX TERMS Arc flash, arc resistance, DC arc flash, ETAP, incident energy, maximum power, NFPA 70E, personal protective equipment.

I. INTRODUCTION

Increasing exposure to DC systems results in increased chances of personnel injury from DC electrical hazards, including arc flash. In 2018, IEEE Std 1584 – *IEEE Guide for Performing Arc-Flash Hazard Calculations*, [1], saw revisions that completely changed the standard based upon additional testing performed to address inadequacies in the original 2002 empirically derived model. However, this update did not include single phase AC or DC arc flash, thereby leaving NFPA 70E *Standard for Electrical Safety in the Workplace*, [2], to address DC arc flash electrical hazard. Unlike the equations developed in IEEE 1584 for three-phase AC systems, the equations in NFPA 70E are theoretical and were not supported with testing. Industry leading software tools for arc flash analysis, such as ETAP [3], develop their analysis techniques based on standards like IEEE 1584 and NFPA 70E.

DC arc flash testing and the results is limited in the public literature. The most notable testing was performed by Kinectrics [4] which found that the NFPA 70E/maximum power method was over-conservative. More recently, testing was performed by EPRI [5] with a PV power supply which found the NFPA 70E/maximum power method was about 3 to 10 times higher than their measured results. Additionally, DC arc flash testing was conducted by AEP utilizing 125 V flooded lead-acid batteries for the arc testing power supply which also found the maximum power method for arcs in an enclosure to be conservative [6], [7].

Prior rectifier supply tests did not use vertical electrodes terminated in an insulating barrier inside a metal box / enclosure (VCBB) electrode configuration. As determined with AC testing and illustrated in [8], the VCBB configuration was deemed more applicable to real electrical equipment, saw increased incident energy and arcing current, decreased arc length, increased arc stabilization, and allowed for more arc sustainability for low voltage AC arc flash during testing when compared to the original vertical electrodes in a metal box / enclosure (VCB) configuration. The VCB configuration was the initial electrode configuration used for arc testing in

This work is licensed under a Creative Commons Attribution 4.0 License. For more information, see https://creativecommons.org/licenses/by/4.0/

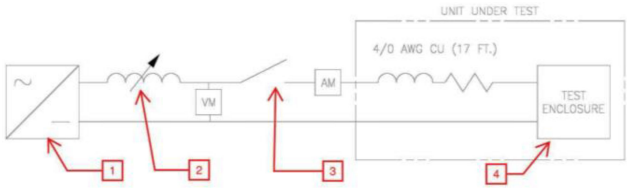


FIGURE 1. Simplified test circuit. Item 1: Rectifier Item 2: Variable Inductor Item 3: Switch Item 4: Arc Flash Test Enclosure.

enclosures, and as illustrated in [9], [10], the VCB configuration yielded higher incident energy than open air due to the reflection of the energy by the enclosure out of the open front.

Reference [4] and [5] highlight the need for additional testing of DC arc flash to ensure that workers are adequately protected, but not unnecessarily over-burdened, with excessively over-conservative personal protective equipment (PPE). For this work, testing was performed at 130 VDC in an attempt to confirm the incident energy results obtained from NFPA 70E and ETAP, and to determine if there is a minimum available short circuit fault current where an arc flash event could no longer occur. For DC system evaluation, it was presumed that the benefits for increased energy results, and observable increases in low voltage sustainability in AC tests with the VCBB configuration would also be applicable for DC tests.

In Section II, the experimental setup and testing procedures are detailed. In Section III, the experimental results are presented. In Section IV, the theoretical models with the parameters of the experimental testing are used to calculate the estimated incident energy. In Section V, the incident energies measured during testing are compared to the estimations from the theoretical models. Finally, in Section VI, conclusions are drawn based upon the results of the comparison.

II. EXPERIMENTAL SET-UP AND TEST PROCEDURE

As stated, the main purpose of performing our experiments is to determine for what system characteristics, if any, an arc is possible for DC based electrical systems. Testing was performed at 130 VDC with multiple fault currents, and bus gap distances. Bolted fault current varied from 1.9 kA to 27.5 kA, and bus gap distance varied from 12.7 mm (0.5 in) to 63.5 mm (2.5 in). The time constant of the system varied slightly with fault current due to the nature of the test circuit and ranged from 10.7 to 17.4 ms.

The test circuit, Fig. 1, consists of a rectifier as the power supply, variable inductor (impedances changed based on the taps used) to set the time constant of the circuit, voltmeter, switch, ammeter, and the circuit under test. The rectifier was supplied by AC power through the lab's generators. The voltage after the inductor, but before the switch, is measured. Since the voltage is measured just before the unit under test, the arcing voltage V_{arc} could easily be obtained. The current is measured on the load side of the switch, before the unit under test to obtain the arcing current I_{arc}, as seen in Fig. 1.

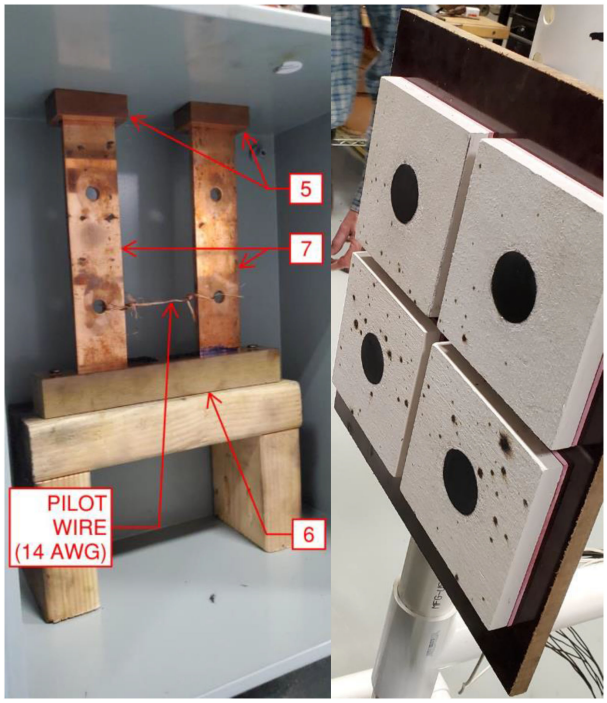


FIGURE 2. Test enclosure for arc flash test with pilot wire (left), ASTM F1959 monitor sensors calorimeter array (right). Item 5: Bus Entry Garolite Insulator Blocks Item 6: Garolite Termination Insulator Block Item 7: Bus Bars.

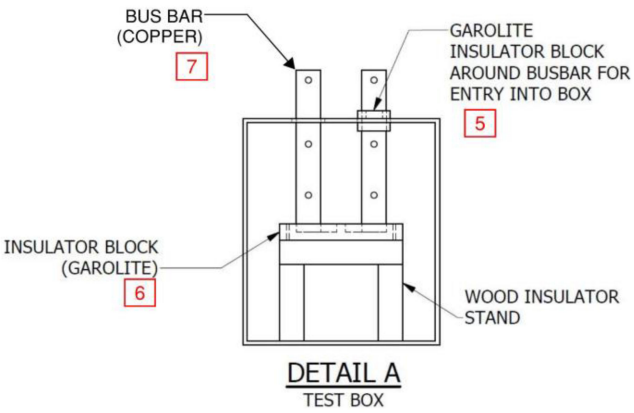


FIGURE 3. CAD detail of test enclosure.

The circuit under test consists of cables from the lab's DC bus to the arc flash test enclosure. The arc flash test enclosure, Fig. 2 and 3, consists of copper bus bars, that are shorted together with a 14 AWG pilot wire, an insulating barrier that the bus bars sit into, and an insulating stand that holds the barrier up from the bottom of the enclosure. The pilot wire is used to initiate the short circuit fault current path. Due to the high levels of fault current, the small gauge wire melts like a fuse, and if the energy is sufficient enough to create and sustain the arc, an arc flash will occur. A longer time constant allows more energy to be transferred [12] and therefore increases the

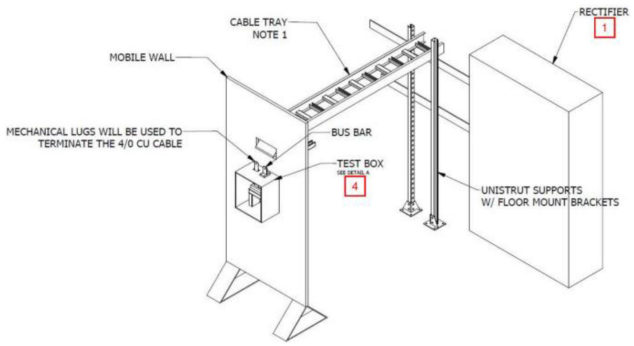


FIGURE 4. CAD model of test setup.

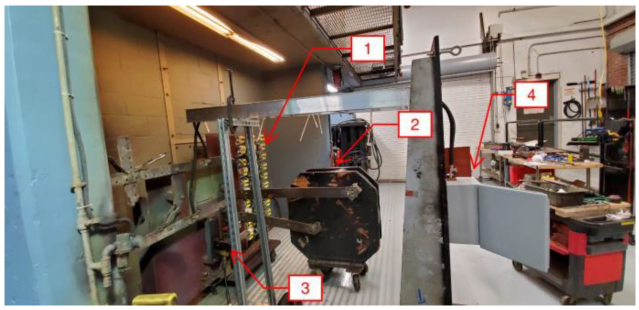


FIGURE 5. Testing lab test setup.

probability of a sustainable arc flash. In front of the open-front enclosure, a calorimeter array, shown in Fig. 2, is placed to measure the heat that is produced by a successful arc flash event.

A. TEST SETUP

More specifically, in Fig. 4 and 5, the circuit under test consists of 4/0 copper 2 kV RHW2 cable, about 4.57 m (15 ft) lengths, routed via one section of aluminum cable tray from the lab's DC bus to the mobile wall. The conductor passed through the mobile wall and terminated at the bus bars entering the enclosure, using mechanical lugs. The bus bars were rectangular copper bars, 6.35 mm (0.25 in) thick, 38.1 mm (1.5 in) wide, in a side-by-side configuration, as seen in Fig. 2 and 3. The bus bars were shorted during testing by bare 14 AWG stranded copper pilot wire. The distance from the back of the bus bars to the back of the enclosure was 47.625 mm (1.875 in).

Insulating barriers made of Garolite were premade prior to testing. Two types of insulators were manufactured. One for the bus entry into the test enclosure, and the other was the termination insulating barrier as seen in Fig. 2 and 3. The termination insulating barrier was 38.1 mm (1.5 in) wide, 190.5 mm (7.5 in) long, and 25.4 mm (1 in) thick. The barrier had 6.35 mm (0.25 in) wide, 12.7 mm (0.5 in) deep, slots milled into the center to allow for the bus to set into the insulating block, creating the VCBB configuration, and still

TABLE 1 Testing Parameters

Factor	Levels
Gap Distance	12.7, 25.4, 38.1, 50.8, 63.5 mm (0.5, 0.75, 1.0, 1.5, 2.5 in)
System Voltage	130 VDC Stiff Source
Bolted Fault Current	1.9, 7.4, 12, 15.8, 20.9, 27.5 kA
L/R	10.7, 11.0, 11.1, 12.0, 13.5, 17.4 ms

Test Current must reach 99% of I_{SC} in five (5) time constants and sustain I_{SC} for 200 ms.

allowed for the gap distance to be varied. The insulating barrier was secured to the wooden insulating support, with the top of the insulator 158.75 mm (6.25 in) from the top of enclosure. The entry insulator was fashioned in a T-shape, allowing the bus to be insulated above and below the top of the enclosure.

There were five, 355.6 mm (14 in) × 304.8 mm (12 in) × 203.2 mm (8 in) metallic ungrounded enclosures with bus entries at the different bus gap spacing, listed in Table 1, in the top that accepted the Garolite entry insulators. The entry insulators were compression fit in the openings of the enclosure and did not require bolting onto the enclosure. The enclosures largely set the gap distance, while the slots of the insulating barrier allowed free movement between the different enclosures. 3M Scotchfil insulating putty was used to fill the additional slot opening not filled by the copper bus bar. The putty is rated for 600 V and a temperature rating of 0 to 80 °C (32 to 176 °F).

The four (4) calorimeter array, Fig. 2, was mounted on a polyvinyl chloride (PVC) structure. The PVC structure was then secured to the mobile wall such that the calorimeter array was 457.2 mm (18 in) from the bus bars. This value will be referred to as the working distance, which is the distance from the arc to a worker's head/chest. The PVC structure was adjustable to allow the top row of calorimeters to be centered at approximately the top of the insulating barrier. Based on the AC testing of the VCBB configuration in [8], if an arc was sustainable, it was believed that it would also occur just above the insulating barrier. Therefore, it was desirable to have a calorimeter centered on this elevation to capture the heat from the arc flash event. The calorimeters were manufactured according to ASTM F1959 standard [11], as a monitor sensor. The calorimeters consist of a copper disk, thermocouple, and sensor holder. The copper disks are 18 g, 101 grade copper, 40 mm diameter, 1.6 mm thick, and have a high-temperature flat black coating with an absorptivity of 0.9 or greater. The thermocouples are 30 AWG, type K thermocouples. The sensor holder is 127 mm (5 in) × 127 mm (5 in) and 12.7 mm (0.5 in) thick made from insulation board that has a density of 737 kg/m^3 (46 lbs/ft^3), and thermal conductivity of 12 W/m·K per ASTM C 177. The insulation board is backed by a 3.175 mm (1/8") thick Arc-Resistant GPO3 fiberglass sheet, to secure the wire, and was adhered to the insulation board with high-temperature (343 °C) silicon adhesive.

TABLE 2 Test Setup Physical Parameters and Dimensions

Test Material	Details
Enclosure Size	355.6 × 304.8 × 203.2 mm (14 × 12 × 8 in)
Electrode Configuration	VCBB
Bus Bars	6.4 mm thick, 76.2 mm wide (0.25 in thick, 1.5 in wide)
Insulating Barrier	38.1 × 190.5 × 25.4 mm (1.5 × 7.5 × 1 in)
Working Distance	457.2 mm (18 in)
Pilot Wire	14 AWG

The thermocouples were terminated to extension wires that entered the control room. The thermocouples were terminated on the data acquisition device (DAQ). The DAQ was an 8-channel USB powered Data Translation DT9828. The module came with its own Omni Software for drivers, and a data logging application QuickDAQ, which was used to capture the temperature readings. The DAQ sampled the temperature readings at 150 Hz for all four thermocouples simultaneously.

To summarize, the overall test setup can be seen in Fig. 4 and 5, and the physical parameters, as detailed above are summarized in Table 2. Testing factors, gap distance, system voltage, bolted fault current, and L/R ratio, and levels, varying values of the factors, were based on a 125 VDC battery supplied control system in an electric generating facility. The factors and their corresponding levels are detailed in Table 1.

The enclosure size, gap distance, and working distance were all based on the IEEE 1584 for panelboards. The electrode configuration was chosen based on the 2018 edition of IEEE 1584; typical DC control system equipment, and the configuration that would yield the highest incident energy. The VCBB configuration is applicable to battery chargers and distribution panelboards, since the conductors are terminating into terminals for the overcurrent protective device, and other equipment where the conductors enter a terminal block.

The system voltage was selected based on the desire to test 125 VDC systems; however, it was common to see battery chargers output 130 VDC, and subsequently the battery banks. Therefore, it seemed prudent to test at this higher DC voltage.

The available bolted fault current for the testing was based on a lead acid battery bank short circuit capabilities. The range was based on the minimum (0.5 kA) and maximum (27 kA) of the entire lineup of a manufacturer's line of Valve-Regulated Lead-Acid (VRLA) and Vented Lead-Acid (VLA) batteries currently installed at the subject generating station.

The L/R ratios were determined using suggestions from [12], which presented common time constants for different systems/equipment types. Reference [12] stated that for control systems the time constants were 10 ms or less, while UPS and battery systems tended to be lower, usually less than 5 ms. The 10 ms time constant was chosen as the nominal value, since a larger time constant allows for more energy to be transferred. The arc clearing time was set to 200 ms, however, it was possible for arcs to self-extinguish before the 200 ms.

The working distance was set based on IEEE 1584 where the typical working distance was 18 inches for panelboards, junction boxes, MCCs, and other equipment. This also encompasses the large majority of DC equipment. The standard's minimum testing distance is 12 inches, since any closer would put the worker in the contact with the arc blast (arc cloud and plasma), however, that is not a defined typical working distance for electrical equipment, and therefore was not included.

The minimum gap distance of 12.7 mm (0.5 in) was based on the minimum allowable spacing between conductors of opposite polarity up to 125 V for switchboards per UL 891 [13].

B. TEST PROCEDURE

The testing performed was a sensitivity analysis with respect to the fault current and gap distance. In general, the tests were performed such that the bus gap distance was increased or decreased at each fault current level depending upon the sustainability of the arc. For an un-sustained test, the gap distance was decreased, and for a sustained test, the gap distance was increased. Once testing was performed at each bus gap, as needed, the bolted fault current was increased or decreased based on the arc's sustainability. If at any gap distance the arc flash event was sustainable, the bolted fault current was decreased. If the bolted fault current was not sustainable at any bus gap distance, then the bolted fault current was increased within the bolted fault current range listed in Table 1.

At each new bolted fault current, a calibration test, where the arc flash enclosure bus bars are shorted with an additional bus bar was performed at the new fault current to ensure that the desired L/R ratio and bolted fault current was reached. The calibration tests were repeated as needed to reach the desired L/R ratio and bolted fault current.

Testing started at the middle of the bolted fault current range listed in Table 1, at 12 kA with an L/R ratio of 10.7 ms. The testing was started in the middle in order to decrease the number of iterations required when trying to find if there was a minimum fault current for arc flash occurrence. If at 12 kA and any gap distance in the range, the test always sustained then no further testing above 12 kA is required. If it never sustained, then testing would not be required below 12 kA.

The fault current was increased/decreased at intervals of approximately 5 kA until the fault current level was about 2 kA, or the maximum fault current, 27 kA, was reached. See Table 1 for the fault current levels and corresponding L/R ratios used during testing.

In the event that an arc flash event did not occur, the test was repeated at least one additional time to ensure the arc flash event still did not occur. If an event occurred after the first re-test, no additional tests were required for sustainability, and the standard testing process was resumed. In the event that an arc flash still did not occur on a retest, the gap distance was



FIGURE 6. Bus bar erosion.

decreased by about 12.7 mm (0.5 in) increments, to the values listed in Table 1 and performed at the same fault current.

After each failed test, the insulating barrier was cleaned using a wire brush and wiped clean with a shop towel. The insulating putty was replaced as needed. The 3M putty was flammable and sometimes caught fire, typically only on a successful arc flash event. The pilot wire was replaced and then the test was repeated.

On a repeated test with a failure, the test box was replaced with the next smaller gap distance, and the insulating barrier and bus bars were cleaned before testing.

On a successful arc flash event, the test box was replaced with the next larger gap distance. The insulating barrier was generally replaced, due to damage sustained from the arc flash event. Insulators that were salvageable were cleaned using a wire brush and shop towel. After cleaning they were ohmed to ensure that the insulating barrier was still acceptable and not impregnated with electrode material from the arc flash event. The bus bars were eroded during testing, as seen in Fig. 6, and were replaced or flipped after a successful test to keep a flat edge at the bus gap. Bus bars that were salvageable to be flipped, were cleaned with wire brush, file, and abrasive pads, as needed. Excess copper that melted and prevented the bus bar from fitting in the insulating barrier slot, was removed to obtain the full depth of the insulator.

III. TEST RESULTS

A list of tests with the fault current, gap distance, time constant, and outcome is shown in Table 3. In Table 3 test numbers 1, 12, 14, 16, 23, and 27 are not shown since they were calibration tests only. A table indicating the outcome of the sustainability, incident energy, and the test parameters is shown in Table 4. Note that only one test resulted in an incident energy over 1.2 cal/cm^2.

The copper bus bars experienced significant erosion for tests that were sustainable. Bus bar erosions measured over 12.7 mm (0.5 in). Test 30 had the highest erosion with bus bar erosion measuring approximately 15.9 mm (0.6 in), as seen in Fig. 6.

A. ARC FLASH SUSTAINABILITY

Table 3 and Table 4 show that arc flash events were sustainable through the entire available fault current range tested. In [1], the authors state, "Sustainable arcs are possible but less likely in three-phase systems operating at 240 V nominal or less with an available short-circuit current less than 2000 A." Hence, it was expected that a minimum fault current would be discovered where it would not be possible to have a sustainable arc flash event. However, such a conclusion could not be made for

TABLE 3 Test Outcomes

Test No.	Bus Gap (mm) [in]	I_{bf} (kA)	Time Constant (ms)	Test Result
2	12.7 [0.5]	12	10.7	Sustained
3, 4, 5	63.5 [2.5]	12	10.7	Un-sustained
6, 7, 8	38.1 [1.5]	12	10.7	Un-sustained
9, 10, 11	25.4 [1]	12	10.7	Un-sustained
13	12.7 [0.5]	7.4	11.1	Sustained
15	12.7 [0.5]	1.9	12.0	Sustained
17, 18, 19	38.1 [1.5]	20.9	13.5	Un-sustained
20	25.4 [1]	20.9	13.5	Un-sustained
21	25.4 [1]	20.9	13.5	Sustained
22	25.4 [1]	20.9	13.5	Sustained
24	19.1 [0.75]	15.8	11	Sustained
25	25.4 [1]	15.8	11	Un-sustained
26	25.4 [1]	15.8	11	Sustained
28	25.4 [1]	27.5	17.4	Un-sustained
29	25.4 [1]	27.5	17.4	Sustained
30	12.7 [0.5]	27.5	17.4	Sustained
31	38.1 [1.5]	27.5	17.4	Un-sustained

Missing test numbers are calibration tests which are not included.

TABLE 4 Test Result Summary

I_{bf} (kA)	Bus Gap (mm) [in]					Time Constant (ms)
	12.7 [0.5]	19.1 [0.75]	25.4 [1]	38.1 [1.5]	63.5 [2.5]	
1.9	0.52*	**				12.0
7.4	0.67*	**				11.1
12	0.80*		*	*	*	10.7
15.8		0.72*	0.66*			11.0
20.9			0.85, 0.70*	*	**	13.5
27.5	1.87*		0.97*	*	**	17.4

I_{bf} = Bolted Fault Current
#* = Incident Energy (cal/cm2) Measured, Actual Test
** = Predicted Result
Green Shading Indicates Sustained
Red Shading Indicates Un-sustained

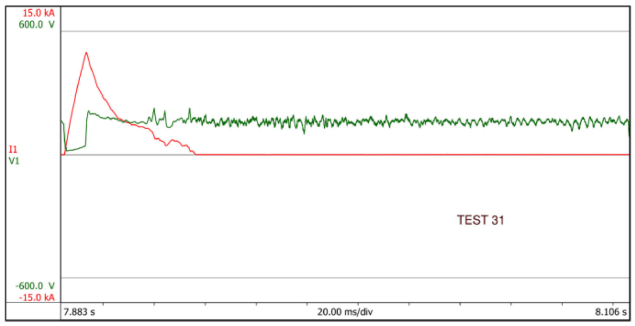


FIGURE 7. Test 31, un-sustained arc flash event, fault current (red) and voltage (green) waveforms. 38.1 mm (1.5 in) gap distance, 17.4 ms time constant, and 27.5 kA bolted fault current.

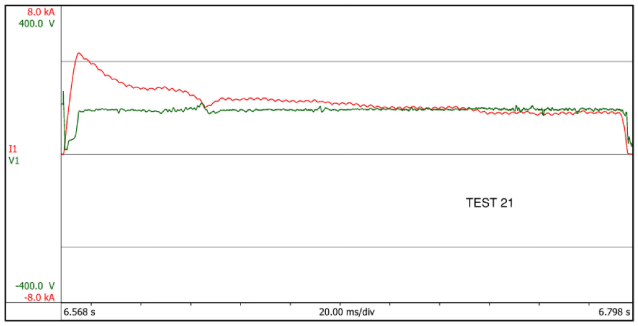


FIGURE 8. Test 21, sustained arc flash event, fault current (red) and voltage (green) waveforms. 25.4 mm (1 in) gap distance, 13.5 ms time constant, and 20.9 kA bolted fault current.

125/130 V DC systems. If the 125 V DC equipment is limited to a minimum of a 25.4 mm (1 in) bus gap, then a similar statement could be made for 125/130 V DC systems. As seen in the testing at 12 kA, it was not possible to sustain an arc flash event at the 25.4 mm (1 in) bus gap on three separate trials.

It is interesting to note that no arc flash event was sustainable beyond the 25.4 mm (1 in) gap. Even at the maximum fault current tested at 27.5 kA, the 38.1 mm (1.5 in) gap was not sustainable. It self-extinguished rapidly, ending approximately 45 ms after the pilot wire was melted as seen in Fig. 7. This was at least twice as long as the other non-sustaining 38.1 mm (1.5 in) gap tests.

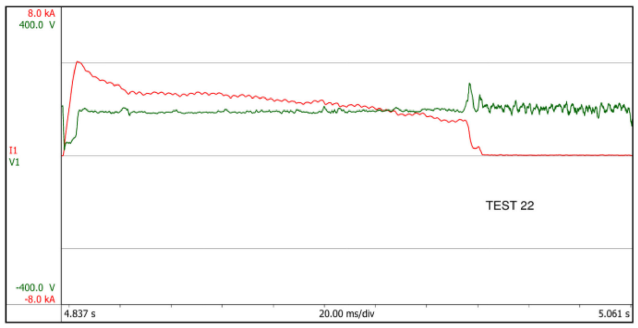


FIGURE 9. Test 22, self-extinguishing sustainable arc flash event, fault current (red) and voltage (green) waveforms. 25.4 mm (1 in) gap distance, 13.5 ms time constant, and 20.9 kA bolted fault current.

B. GAP DISTANCE IMPACT ON INCIDENT ENERGY LEVELS

As seen by the un-sustainability of an arc flash event at gap distances beyond the 25.4 mm (1 in) bus gap, it is clear that gap distance has a large impact on sustainability. In addition, gap distance also has a large impact on the incident energy. It was found that incident energy was inversely proportional to the gap distance. As seen in Table 4, the incident energy of a 12.7 mm (0.5 in) gap at 12 kA was 0.80 cal/cm^2. While the incident energy of a 19.1 mm (0.75 in) gap at 15.8 kA had a lower incident energy of 0.72 cal/cm^2. Increasing the gap distance by only 6.35 mm (0.25 in) caused the incident energy to be lower even with an additional 3.8 kA available fault current. Two other examples showing the impact of gap distance are the tests occurring at 15.8 kA and 27.5 kA. At 15.8 kA bolted fault current, the bus gap was increased by 33% (19.1 mm (0.75 in) to 25.4 mm (1 in)) causing an 8% decrease in the incident energy (0.72 to 0.66 cal/cm^2). At 27.5 kA bolted fault current, the bus gap increased by 100% (12.7 mm (0.5 in) to 25.4 mm (1 in)) causing a 48% decrease in the incident energy (1.87 to 0.97 cal/cm^2).

C. PEAK FAULT CURRENT IMPACTS ON SUSTAINED ARCS

In three instances an arc flash event sustained on the second trial of a test after it did not sustain on the first trial, all of which were at a 25.4 mm (1 in) bus gap. For test 20 the arc did not sustain. However, the next test with the same parameters, test 21, the arc did sustain with fault current initially falling steadily after the pilot wire melted before flattening out around 2.2 kA at about 170 ms into the test, as seen in Fig. 8. Since this was the first experience when an arc flash event occurred after an un-sustaining event, the same conditions were re-evaluated. In test 22, an arc flash event occurred, however, it self-extinguished around 160 ms after the pilot wire melted, as seen in Fig. 9. In comparison to test 21 in Fig. 8, they both decrease steadily after the pilot wire melts. However, in test 21 the current flattens out at around 125 ms after the pilot wire melts while for test 22 the current exponentially decays. At about 152 ms, after the pilot wire melts, the current collapses and is extinguished at about 159 ms, after the pilot wire melts.

One contributing factor to the difference between the results of test 21 and 22 is the peak current. The current peaked at 5.5 kA for test 21 while the current only peaked at 5.1 kA for test 22. Both of these tests had current peaks that were relatively close, unlike the un-sustaining event that had a current peak of 7.6 kA. The experiments show that at a much higher peak current, 7.6 kA, the arc did not sustain while at a lower current, 5.5 kA, the arc did. However, the slightly lower current, 5.1 kA, did not sustain the entire duration.

To further explore the coupling between peak fault current and arc sustainability, a few additional tests were run to gather additional observations. Tests 25 and 26 utilized a 25.4 mm (1

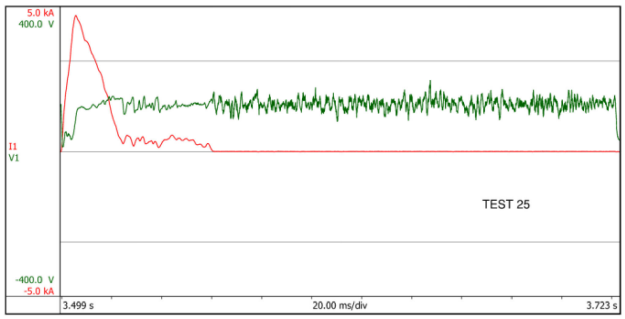


FIGURE 10. Test 25, un-sustained arc flash event, fault current (red) and voltage (green) waveforms. 25.4 mm (1 in) gap distance, 11 ms time constant, and 15.8 kA bolted fault current.

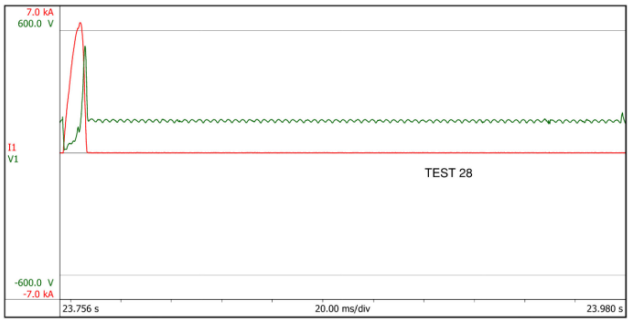


FIGURE 12. Test 28, un-sustained arc flash event, fault current (red) and voltage (green) waveforms. 25.4 mm (1 in) gap distance, 17.4 ms time constant, and 27.5 kA bolted fault current.

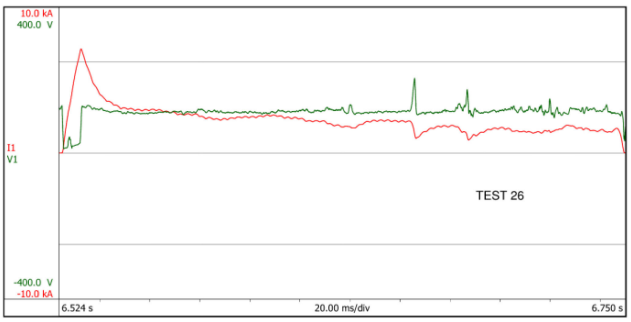


FIGURE 11. Test 26, sustained arc flash event, fault current (red) and voltage (green) waveforms. 25.4 mm (1 in) gap distance, 11 ms time constant, and 15.8 kA bolted fault current.

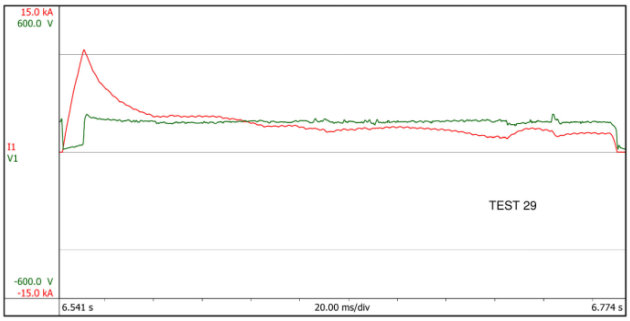


FIGURE 13. Test 29, sustained arc flash event, fault current (red) and voltage (green) waveforms. 25.4 mm (1 in) gap distance, 17.4 ms time constant, and 27.5 kA bolted fault current.

in) bus gap, and a *bolted fault current of 15.8 kA*. Test 25, Fig. 10, did not sustain, while the retest, test 26 in Fig. 11, did.

For test 25, the peak current reached 4.7 kA, at which point the pilot wire melted. After melting, the current decreased rapidly, dropping to about 280 A in 19 ms, and the current reached zero 55 ms after the pilot wire melted.

For test 26, the arc sustained with the fault current decreasing rapidly after the pilot wire melts, as typically seen, and flattening out around 2.5 kA. Additionally, at about 134 ms and 155 ms after the pilot wire melts, the current sharply decreases as if about to extinguish, similar to what is seen in test 22, however, in this test case the current recovers both times and sustains the arc.

Tests 28 and 29 utilized a 25.4 mm (1 in) bus gap, and a *bolted fault current of 27.5 kA*. Test 28, Fig. 12, did not sustain, while the retest, test 29 in Fig. 13, did. On test 28 the peak current reached 6.2 kA, at which point the pilot wire melted. After melting, the current decreased very rapidly, dropping to about zero in about 3.1 ms.

Test 29 sustained with the fault current decreasing rapidly after the pilot wire melts and flattening out to around 3.6 kA in about 29 ms. After the pilot wire melts, the current settles to 2.5 kA after 130 ms have passed. Additionally, at about 175 ms and 195 ms after the pilot wire melts, the current decreases as if it were to extinguish, similar to what has been seen in test 26. However, in this test case, the current did not decrease as rapidly as seen in test 26.

Observing these three testing groups the largest difference between each set of tests is the peak current. For tests 20 through 22, the peak currents were 7.6 kA, 5.5 kA, and 5.1 kA respectively. Unsurprisingly, the higher peak current resulted from the time it took for the pilot wire to melt. The result that is surprising is that the highest peak current was the test that was unable to sustain, while the other two tests had lower currents and were able to sustain for most, or all, of the test. In addition, the peak current of test 22 was only about 380 A less than test 21, however, test 21 was able to sustain the entire test duration of 200 ms, while the slightly lower test 22 did not. For tests 25 and 26, the opposite occurred. Tests 25 and 26 had peak currents of 4.7 kA, and 7.1 kA respectively. In this case the higher peak current was able to sustain, while the lower was not. Tests 28 and 29 had peak currents of 6.2 kA and 10.5 kA respectively. Again the higher peak current (longer time taken for the pilot wire to melt) test sustained while the lower peak current did not.

As stated earlier, all three of these tests groups had the second test sustain while the first was un-sustained. This can be attributed to excess carbon and copper that remained after the first test. Although the insulating barrier, and bars, were cleaned between tests, not all products from the arc can be

removed by normal means. Having the excess conductive material during the test would make the arc more likely to sustain. This presence of conductive material within the equipment, however, would be more representative of typical industrial installations. Electrical equipment, especially in steel mills, power plants and other heavy industrial facilities, would not be in pristine condition even after a maintenance outage. Since access to bars, terminals and other current carrying parts within the gear is virtually impossible to clean to the level in the lab, the existence of conductive dusts and materials in the switchgear presents an increased likelihood of a sustained arc when a fault has occurred.

IV. INCIDENT ENERGY RESULTS BASED ON THEORETICAL EQUATIONS

Theoretical models were created/utilized to compare with the experimental results. The theoretical models used were the NFPA 70E – 2015 [14], NFPA 70E – 2018 [2], and maximum power, Stokes and Oppenlander, and Paukert methods using ETAP 19.5.0. There are additional theoretical models as summarized in [15], but these five methods are the focus for the comparative analysis.

The NFPA 70E, Standard for Electrical Safety in the Workplace, establishes requirements and guidelines to address the safety of employees exposed to electrical hazards, in particular interacting with energized equipment, in order to create a safe environment for employees either performing maintenance or general workplace electrical safety practices. In article 130.5 of NFPA 70E – 2018, addressing arc flash risk assessment, if the use of PPE is deemed necessary after a risk assessment, the NFPA 70E – 2018 allows for the use of one of the two different methods of determining appropriate PPE for workers, but not both. Either the incident energy analysis method or the arc flash PPE category method can be used as per Article 130.5(F).

The incident energy analysis method takes into consideration the working distance, the overcurrent protective device, equipment condition, and fault clearing time (as per Article 130.5(G)), and the PPE is selected using Table 130.5(G), which is split into two incident energy exposure categories (1.2 to 12 cal/cm^2 and greater than 12 cal/cm^2). Informative Annex D has information regarding the calculation of both AC and DC incident energy calculations. DC incident energy calculation methods are detailed in Section D.5. Section D.5.1 is based on the maximum power method developed by Doan [16]. Doan estimated the maximum power of the arc by having the arcing resistance equal to the system resistance and then developed an equation of the incident energy based on the clearing time and working distance. This approach is very similar to the method developed by Lee for AC systems [17], which was also based on the maximum power of an arc based on the available short circuit current, to find the maximum theoretical model of radiant heating from an arcing fault. Per Section D.5.1, the arcing current is calculated with (1) and used to calculate the incident energy, (2).

$$I_{arc} = 0.5 \times I_{bf} \tag{1}$$

$$IE_m = 0.01 \times V_{sys} \times I_{arc} \times T_{arc}/D^2 \tag{2}$$

Where,

I_{arc}= arcing current (A)
I_{bf} = system bolted fault current (A)
IE_m = estimated DC arc flash incident energy at the maximum power point (cal/cm^2)
V_{sys} = system voltage (V)
T_{arc} = arcing time (s)
D = working distance (cm)

If the arc is in a box, or enclosure, the standard recommends to consider PPE that is beyond the requirements of the PPE category method. This is different than the previous recommendation of multiplying the result of (2) by a factor of three in the 2015 edition for arcs in an enclosure. A bias or factor does seem prudent to add, based on the findings in [9] and [10] for AC arc flash testing.

The maximum power method is also recommended by the National Electrical Safety Code [18], which provides guidelines to protect workers and facilities of utilities, thereby solidifying Doan's method to be the most accepted method in industry for calculating incident energy for DC arc flash. However, there are many sources, [19]–[22] that have illustrated the differences between PV systems and other DC systems, namely its non-linear I-V characteristic, and the close proximity of the short circuit current and normal operating point. Most of the references state that the typical maximum power transfer method developed by Doan is not applicable to PV systems. PV system arc flash testing has been performed, and in [5] concluded that no theoretical model adequately quantifies the incident energy.

The PPE category method, Article 130.7(C)(15), is applicable for AC and DC systems of specified parameters, such as voltage, available fault current, equipment type, working distance, and arc duration. If the parameters are outside of those specified, this method cannot be used and the incident energy calculation method must be used. For DC systems, Table 130.7(C)(15)(b) is used. The PPE category tables (task tables) classify PPE into four categories (Category 1 through 4) corresponding to arc clothing ratings of 4 cal/cm^2, 8 cal/cm^2, 25 cal/cm^2, and 40 cal/cm^2 respectively, and additional necessary ancillary equipment such as hard hats, hearing protection, leather gloves, etc. which also vary based on the level of incident energy.

In the testing performed, only the tests that were below 15 kA bolted fault current are applicable to use the PPE category method.

The results of (2), the 2015 factor of 3 method, and the 2018 method for arcs in an enclosure for each test method are listed in Table 5. The working distance for all tests were 45.72 cm (18 in), the system voltage was 130 V, and the arcing time was 200 ms. It is important to note that none of these

TABLE 5 NFPA 70E – 2015 and 2018 Methods

I_{bf} (kA)	I_{arc} (kA)	IE_m (cal/cm^2)	NFPA 70E – 2015 IE Rating (cal/cm^2)	NFPA 70E – 2018 IE Rating (cal/cm^2)
1.9	1.0	0.12	0.35	8
7.4	3.7	0.46	1.38	25
12	6	0.75	2.24	25
15.8	7.9	0.98	2.95	N/A
20.9	10.5	1.30	3.90	N/A
27.5	13.8	1.71	5.13	N/A

I_{arc} = Arcing Current
IE_m = Incident Energy at Maximum Power Point from (2)
IE = Incident Energy
NFPA 70E – 2015 is with the factor of three for enclosures
NFPA 70E – 2018 are the values specified by the task tables to be used for arcs in an enclosure. Values marked N/A exceed the parameters for the task tables and therefore the tables cannot be used.

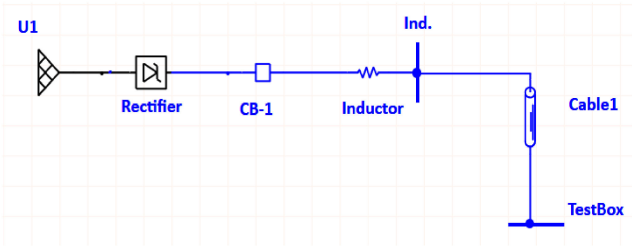


FIGURE 14. ETAP 19.5.0 One-line diagram of test circuit.

methods consider bus gap distance as a factor in determining incident energy, but this was seen as an important variable from our experimental trials. It is easy to see from Table 5 that the PPE requirements when selecting PPE from the task tables is much higher than the previous recommendation of multiplying the incident energy result from (2) by three for arcs in an enclosure.

As systems get more complex these calculations become more cumbersome, and therefore power system analysis software is utilized for arc flash analysis/studies. The majority of arc flash studies performed in industry are done using various power system analysis software capable of arc flash analysis such as, ETAP, SKM, EasyPower, etc. ETAP 19.5.0 was used to model the experimental test setup and parameters and obtain arc flash incident energy values using ETAP's available arc flash calculation methods. ETAP has three different DC arc flash methods; maximum power, Paukert, and Stokes and Oppenlander. Paukert's [23], and Stokes and Oppenlander's [24] methods are based on arc resistance. Their findings and a comparison of their results is detailed in [25]. It was concluded that their models generally agreed with each other; however, they did have some deviation especially for larger gap distances. The one-line diagram from ETAP is shown in Fig. 14.

TABLE 6 ETAP 19.5.0 Arc Flash Results

I_{bf} (kA)	Maximum Power (cal/cm^2)	Paukert (cal/cm^2)	Stokes & Oppenlander (cal/cm^2)
1.9	0.35	0.16	0.17
7.4	1.38	0.67	0.66
12	2.24	1.08	1.06
15.8	2.95	1.07	1.29
20.9	3.90	1.32	1.50
27.5	5.13	2.40	2.32

The TestBox bus, is modeled as the test enclosure mounted on the mobile wall. The settings of the box were changed to match those of the test enclosure, such as the equipment properties, and conductor/electrode properties. The settings input were: equipment type as panelboard, box was checked, the test setup enclosure dimensions were input, reflectivity coefficients were left at the default values, the gap between conductors was set at the minimum values used during testing at each fault current level, 12.7 mm (0.5 in), 19.1 mm (0.75 in), and 25.4 mm (1 in), conductor orientation was set to vertical, the termination was set to insulating barrier, and the conductor type was set to copper. Cable1 is modeled as the 4.57 m (15 ft) 4/0 copper cable that was routed via cable tray from the DC bus to the test enclosure.

The test circuit inductor was modeled as a DC impedance with resistance and inductance values to obtain the L/R ratio for each test setup. Since the experimental test setup had a protective device for disconnecting power after 200 ms to the test circuit on the AC side it was necessary to add a DC circuit breaker CB-1 to the circuit. A DC circuit breaker without an instantaneous setting and a short-time pickup long enough to not trip in 200 ms was selected. The arc flash study fault clearing time setting was changed to limit the maximum fault clearing time to 200 ms. Alternatively, the protective device could be excluded if the TestBox bus, arc flash user-defined source protective device, setting was changed to use a fixed fault clearing time. Lastly, the rectifier was modeled to provide the bolted fault current for each test setup, by varying the short circuit contribution.

The analyses were run for each test scenario with all three of the different arc flash methods available by ETAP 19.5.0. The results are listed in Table 6.

V. COMPARISON OF INCIDENT ENERGY MODELS WITH EXPERIMENTAL RESULTS

The testing data was compared to the results obtained from the NFPA 70E methods, as consolidated in Table 7.

When the NFPA 70E – 2018 PPE category method is used, the minimum arc rating of PPE was about 15 to 35 times higher than the incident energy measured during testing. This is illustrated in Fig. 15.

TABLE 7 Test Results and NFPA 70E – 2015 and 2018 Methods

I_{bf} (kA)	IE Measured (cal/cm^2)	IE_m (cal/cm^2)	NFPA 70E – 2015 IE Rating (cal/cm^2)	NFPA 70E – 2018 IE Rating (cal/cm^2)
1.9	0.52	0.12	0.35	8
7.4	0.67	0.46	1.38	25
12	0.8	0.75	2.24	25
15.8	0.72	0.98	2.95	N/A
20.9	0.85	1.30	3.90	N/A
27.5	1.87	1.71	5.13	N/A

IE Measured = Maximum Incident Energy Measured During Testing (at fault current level)
NFPA 70E – 2015 is with the factor of three for enclosures
NFPA 70E – 2018 are the values specified by the task tables to be used for arcs in an enclosure. Values marked N/A exceed the parameters for the task tables and therefore the tables cannot be used.

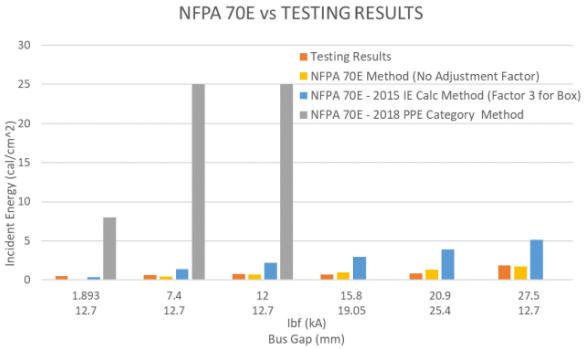


FIGURE 15. Incident energy comparison between testing results and NFPA 70E methods including 2018 PPE category method at bolted fault currents tested. Gap distance listed below fault current only applies to the test results, NFPA 70E methods do not consider bus gap in incident energy determination.

When using the incident energy calculation from informative annex D from NFPA 70E, the standard recommends that the task table be used and that PPE ratings selected be beyond what the table recommends resulting in even higher PPE incident energy ratings for arcs in an enclosure. This provides an even larger disparity between the recommended PPE and the test results. In addition, this recommendation effectively eliminates the incident energy analysis method when the arc occurs in an enclosure. The 2018 NFPA 70E also neglects to address situations where the fault current is beyond the PPE category method limits and the arc is in an enclosure. For cases that exceed the task tables, the incident energy calculation method is to be used; however, for DC systems it references the user back to the task tables. Since no recommendation is provided for cases that are above 15 kA, and are in an enclosure, to err on the side of caution would be to prohibit work on the equipment while energized. Comparing the recommendation of the 2018 NFPA 70E to the actual test results yield of less than 2 cal/cm^2, at the maximum tested fault current of 27.5 kA, indicates that the use of the task

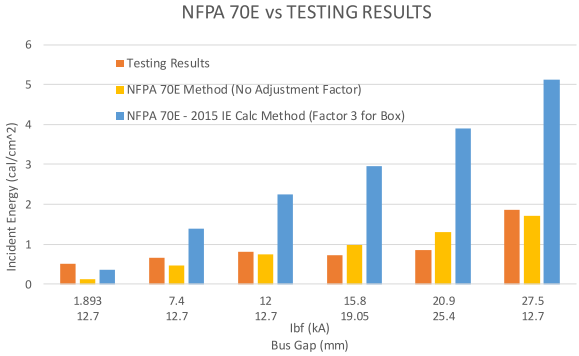


FIGURE 16. Incident energy comparison between testing results and NFPA 70E methods (excluding 2018 PPE category table method) at bolted fault currents tested. Gap distance listed below fault current only applies to the test results, NFPA 70E methods do not consider bus gap in incident energy determination.

tables for the incident energy calculation method for arcs in an enclosure should be reviewed based upon further testing. As seen in Fig. 16, the 2015 method's highest minimum PPE rating was 5.13 cal/cm^2 at the 27.5 kA available fault current. This still indicates higher PPE requirements than the test results; however, it is not the drastic changes as seen by the 2018 edition.

Typical arc formation is from the bottom of the electrodes and arc between the electrodes from the bottom, causing the arc to shoot downwards into the bottom of the enclosure and reflect outwards. In the VCBB configuration, however, this arc formation cannot occur resulting in arc formation just above the insulating barrier causing the arc to be directed more outwards than the typical VCB configuration, thus resulting in higher incident energy at the calorimeters. Even in this configuration, which should produce a higher incident energy, the measured results were at least a factor of ten less than the results calculated using the 2018 edition of the NFPA 70E standard. Also, the methods of this standard do not consider bus gap distance as a parameter, and therefore will produce incident energy values at gap distances where it was not possible to sustain an arc during testing.

The previous edition, NFPA 70E 2015, recommends multiplying the calculated incident energy using (2) by a factor of three (3) for enclosures. Since our testing was done inside the box, this recommended factor was applied. As a result, the calculated values were about 2 to 4.5 times higher than those obtained from testing. Except for the test case of 12.7 mm (0.5 in) gap at 1.9 kA bolted fault current, which has about half of the measured incident energy. The largest disparities for the other tests were the 20.9 kA and 15.8 kA tests where the gap distances were at 19.1 mm (0.75 in) and 25.4 mm (1 in) respectively, which would produce lower incident energies than if the gap was 12.7 mm (0.5 in), as seen with the other fault current levels. Assuming the incident energy increased at 12.7 mm (0.5 in) gap, the disparity between this method and the measured results would be closer to a factor of two. However, since the maximum fault current from testing was

TABLE 8 Test Results and ETAP 19.5.0 Methods

I_{bf} (kA)	IE Measured (cal/cm^2)	Maximum Power (cal/cm^2)	Paukert (cal/cm^2)	Stokes & Oppenlander (cal/cm^2)
1.9	0.52	0.35	0.16	0.17
7.4	0.67	1.38	0.67	0.66
12	0.8	2.24	1.08	1.06
15.8	0.72	2.95	1.07	1.29
20.9	0.85	3.90	1.32	1.50
27.5	1.87	5.13	2.40	2.32

not at the 12.7 mm (0.5 in) gap it clearly illustrates the importance that gap distance has on incident energy levels. In addition, if performing a study with equipment that has a 63.5 mm (2.5 in) gap distance, the 2015 NFPA 70E method would still yield 2.24 cal/cm^2, as it did for the 12.7 mm (0.5 in) gap at 12 kA. However, during testing it was not possible to sustain an arc at the 63.5 mm (2.5 in) gap distance.

Disregarding the 2015 and 2018 NFPA 70E adjustments of (2) for arc in an enclosure, the results calculated using (2) are consistently lower than the measured values with tests that had a bus gap of 12.7 mm (0.5 in). As mentioned previously, the NFPA 70E equation does not consider gap distance, and therefore as the testing gap distance changed the disparity of the results increased and decreased. The largest disparity between the measured values and (2) was the testing at 1893 A fault current. The measured result was over four times the estimate of (2). However, the other results were generally much closer to the measured value with the result from (2) being half to 1.5 times the measured value. Unfortunately, the results from (2) were under the measured values when the gap distances were 12.7 mm (0.5 in) which would fail to adequately protect the worker from the incident energy. The instances that (2) was above the measured values were when the gap distances were 19.1 mm (0.75 in) and 25.4 mm (1 in). Knowing that the incident energy increases when the gap distance is reduced at 12.7 mm (0.5 in) it is unlikely that the results from (2) would still remain above the test result. Based on these tests, it is clear that multiplying by a factor of three in the 2015 edition was a wise decision.

The testing data was also compared to the results obtained from ETAP and are consolidated in Table 8. As seen in Fig. 17, the ETAP provided results were relatively close to measured values. Stokes and Oppenlander, and Paukert methods were consistently closer to the incident energy compared to the maximum power method. Their results never reaching twice that of the measured value. However, at the 1.9 kA and the 7.4 kA they were both below the measured value, being less than half for the 1.9 kA and being only 0.01 cal/cm^2 less than the measured for the 7.4 kA. The maximum power method had a similar problem at the 1.9 kA, being about 70% of the measured value. However, for all other test cases it was the highest result by far and ranged from 2 to 4.5 times as much as the measured values for the rest of the tests.

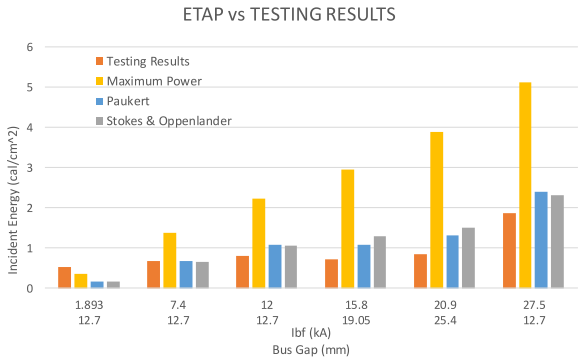


FIGURE 17. Incident energy comparison between testing results and ETAP methods (maximum power, Paukert, and Stokes & Oppenlander) at bolted fault currents tested. Gap distance listed below fault current does not apply to the maximum power method, which is independent of bus gap distance to determine incident energy.

TABLE 9 Comparison of Arc Current Magnitude of NFPA 70E and Experimental Results

Test No.	Bus Gap (mm) [in]	I_{bf} (kA)	Measured Average I_{arc} (kA) [% I_{bf}]	Theoretical I_{arc} (kA)
2	12.7 [0.5]	12	3.0 [25%]	6
13	12.7 [0.5]	7.4	2.4 [32%]	3.7
15	12.7 [0.5]	1.9	0.9 [48%]	1.0
21	25.4 [1]	20.9	2.2 [11%]	10.5
22	25.4 [1]	20.9	3.3 [16%]	10.5
24	19.1 [0.75]	15.8	2.8 [18%]	7.9
26	25.4 [1]	15.8	2.5 [16%]	7.9
29	25.4 [1]	27.5	3.6 [13%]	13.8
30	12.7 [0.5]	27.5	5.2 [19%]	13.8

Theoretical I_{arc} is 50% of I_{bf} per (1).

VI. COMPARISON OF ARC CURRENT MAGNITUDE OF NFPA 70E AND EXPERIMENTAL RESULTS

The NFPA 70E method estimates the arcing current to be half of the bolted fault current as seen in (1). From testing the average measured arcing current ranged from 11 to 48% of the bolted fault current, as seen in Table 9. The disparity between the theoretical estimate and the measured arcing current increases at higher bolted fault currents. Seven (7) of the nine (9) tests were a quarter of the bolted fault current or less. Unsurprisingly, as seen in Table 9, the arcing current reduced as the gap distance increased.

Having an accurate estimation of the arcing current is essential for arc flash incident energy calculations. The magnitude of the arcing current is a key factor in determining the clearing time of the fault. If the arc current is sufficiently low the time to clear could be significantly higher than originally estimated, and could result in an even higher incident energy than originally estimated using (1) and (2).

VII. CONCLUSION

In conclusion, the contribution of this work is to provide further public testing data of DC arc flash, including results of the sensitivity analysis of bus gap and fault current, and to provide a comparative analysis to current theoretical models. From testing it was observed that gap distance has a significant impact on DC arc sustainability and incident energy. The incident energy was found to be inversely proportional to gap distance. In one case, there was a 50% reduction of incident energy when the gap distance was increased from 12.7 to 25.4 mm (0.5 to 1 in). In addition, at gap distances greater than 25.4 mm (1 in), arc flash events were un-sustainable.

The incident energy results obtained from testing differ greatly from the maximum power models. The arc resistance models had some deviation, but were generally closer to the measured incident energies. Generally, these deviations were conservatively high, however, there were a few instances at low fault currents (1.9 kA) where the measured incident energy exceeded the theoretical models. The closeness of results can likely be attributed to the consideration of bus gap in estimating incident energy and the observed large impact gap distance had on incident energy. As stated previously, the arc resistance methods consider bus gap to be a factor in estimating incident energy while the maximum power method does not.

This testing performed and the deviations seen between the measured results and the current theoretical models further cements the need for additional testing to be performed in regards to DC arc flash. The authors recommend that an IEEE standard be developed for DC arc flash. Alternatively, DC arc flash could be added to IEEE 1584 once sufficient empirical data has been collected.

ACKNOWLEDGMENT

The authors would like to thank, Roy Ball, Emmanuel Munguia, and Michael Lang from Mersen in providing lab use, test setup and testing assistance. The authors would like to thank William Weimann III from Wabtec Corporation for acquiring the copper for the bus work, as well as, spending many hours machining all the insulators and bus work used for testing. The authors would like to thank Eric Grant from Eaton Corporation for providing the cable tray, mechanical lugs, and cable for the testing.

REFERENCES

[1] *IEEE Guide for Performing Arc-Flash Hazard Calculations*, IEEE Standard 1584, 2018.
[2] *Standard for Electrical Safety in the Workplace*, NFPA Standard 70E, 2018.
[3] ETAP 19.5 User Guide, Irvine, CA, USA: Operation Technology, Inc., 2019.
[4] K. S. Y. Cheng, S. L. Cress, and D. J. Minini, "Arc hazard assessment for DC applications in the transit industry," in *Proc. APTA Rail Conf.*, Jun. 12-15, 2011, pp. 1–7.
[5] B. Paudyal, M. Bolen, T. Short, and J. Woodard, "Measured and calculated DC arc-flash incident energy in a large-scale photovoltaic plant," *IEEE J. Photovolt.*, vol. 9, no. 5, pp. 1343–1349, Sep., 2019.
[6] A. Gaunce *et al.*, "DC arc flash: Testing and modeling incidents in a 125v substation battery backup system," *IEEE Trans. Ind. Appl.*, vol. 56, no. 3, pp. 2138–2147, May/Jun. 2020.
[7] A. Gaunce *et al.*, "Expanded DC arc flash model for 125V substation battery backup systems," in *Proc. 56th Ind. Commercial Power Syst. Tech. Conf.*, 2020, pp. 1–9.
[8] R. Wilkins, M. Lang, and M. Allison, "Effect of insulating barriers in arc flash testing," in *Proc. Conf. Record 54th Annu. Pulp Paper Ind. Tech. Conf.*, 2008, pp. 120–125.
[9] R. Wilkins, M. Allison, and M. Lang, "Improved method for arc flash hazard analysis," in *Proc. Conf. IEEE Ind. Commercial Power Syst. Tech.*, 2004, pp. 55–62.
[10] R. L. Doughty, T. E. Neal, and H. L. Floyd, "Predicting incident energy to better manage the electric arc hazard on 600-V power distribution systems," *IEEE Trans. Ind. Appl.*, vol. 36, no. 1, pp. 257–269, Jan./Feb., 2000.
[11] *Standard Test Method for Determining the Arc Rating of Materials for Clothing*, ASTM Standard F1959/M1959 – 14, 2014.
[12] H. C. Cline, Fuse protection of DC systems, presented at in Proc. Amer. Power Conf. Annu. Meeting, Apr. 1995, [Online]. Available: https://arcadvisor.com/files/Fuse-Protection-of-DC-Systems.pdf
[13] *Switchboards*. UL Standard 891, 2019.
[14] Standard for Electrical Safety in the Workplace, NFPA Standard 70E, 2015.
[15] T. Gammon, W. Lee, Z. Zhang, and B. C. Johnson, "A review of commonly used DC arc models," *IEEE Trans. Ind. Appl.*, vol. 51, no. 2, pp. 1398–1407, Mar./Apr. 2015.
[16] D. R. Doan, "Arc flash calculations for exposures to DC systems," *IEEE Trans. Ind. Appl.*, vol. 46, no. 6, pp. 2299–2302, Nov./Dec., 2010.
[17] R. H. Lee, "The other electrical hazard: Electric arc blast burns," *IEEE Trans. Ind. Appl.*, vol. IA-18, no. 3, pp. 246–251, May 1982.
[18] 2017 National Electrical Safety Code(R) (NESC(R)). 2017 National Electrical Safety Code(R) (NESC(R)), pp. 1–405, Aug. 2016.
[19] J. Yuventi, "DC electric arc-flash hazard-risk evaluations for photovoltaic systems," *IEEE Trans. Power Del.*, vol. 29, no. 1, pp. 161–167, Feb. 2014.
[20] K. Klement, "DC arc flash studies for solar photovoltaic systems: Challenges and recommendations," *IEEE Trans. Ind. Appl.*, vol. 51, no. 5, pp. 4239–4244, Sep./Oct., 2015.
[21] E. H. Enrique, P. N. Haub, and T. P. Bailey, "DC arc flash calculations for solar farms," in *Proc. 1st IEEE Conf. Technol. Sustain. (SusTech)*, 2013, pp. 97–102.
[22] P. Brucke and M. Manjarekar, "DC arc flash risk assessments for photovoltaic systems," in *IEEE 43rd Photovolt. Specialists Conf.*, 2016, pp. 3234–3236.
[23] J. Paukert, "The arc voltage and arc resistance of LV fault arcs," in *Proc. 7th Int. Symp. Switching Arc Phenom.*, 1993, pp. 49–52.
[24] A. D. Stokes and W. T. Oppenlander, "Electric arcs in open air," *J. Phys. D: Appl. Phys.*, vol. 24, pp. 26–35, 1991.
[25] R. F. Ammerman, T. Gammon, P. K. Sen, and J. P. Nelson, "DC-arc models and incident-energy calculations," *IEEE Trans. Ind. Appl.*, vol. 46, no. 5, pp. 1810–1819, Sep./Oct., 2010.



COREY S. WEIMANN (Member, IEEE) received the B.S. degree in electrical engineering from the Department of Electrical and Computer Engineering, University of Pittsburgh, in 2018. He also received the M.S. degree in electrical and computer engineering from the University of Pittsburgh in 2020. He has worked as an Electrical Engineering Intern with Cintar Inc. from 2013 to 2017 where he traced electrical distribution systems for development of single lines and arc flash studies, and drafting services for various commercial and industrial projects. He worked for the Student Electronics Resource Center (SERC) as an Electronic Technician Intern from 2017 to 2018 where he managed five undergraduate labs, assisted with day-to-day operations, student design projects, and instruction, and provided teaching assistance duties for the course provided by the center. After graduating with the B.S. degree, he returned to Cintar Inc. as Electrical Engineer where he works in various electrical, instrumentation, control, and process roles for heavy industrial projects including; iron ore pelletizing plants, power generation facilities, ore processing facilities, material handling units, and steel mills, and currently serves in that role. He received the Engineering in Training (EIT) certification in Pennsylvania in 2018.



ROBERT J. KERESTES (Member, IEEE) received the B.S. and M.S. degrees from the University of Pittsburgh, 2010 and 2012, respectively, all with a concentration in electric power systems. He received the Ph.D. degree from the Department of Electrical and Computer Engineering, University of Pittsburgh, in 2014. Prior to his education, Robert served in the United States Navy as an Interior Communications Electrician onboard the USS Constellation from 1998 to 2002 and then as a Construction Electrician with the Seabees Naval Construction Battalion from 2002 to 2006. Following his education, Robert worked with Emerson Automation Solutions (formerly known as Emerson Process Management) where he led the development and implementation of mathematical models for electric power applications related to embedded simulation. In 2016, Robert joined the University of Pittsburgh's ECE Department where he focuses on the advancement of pedagogy and assessment in the field of electrical engineering, particularly in the areas of electric power distribution systems, distributed energy resources, and electromagnetism. Robert's research interests include the development of the next generation of electric power distribution systems and the integration of renewable energy resources into the distribution sector. Robert took on the role of Director of the Electrical Engineering Undergraduate Program in the Spring of 2017 and currently serves in that role.



BRANDON M. GRAINGER (Senior Member, IEEE) received the bachelor's degree in mechanical engineering (with minor in electrical engineering) and master's degree in electrical engineering from the University of Pittsburgh. He received the Ph.D. degree in electrical engineering with a specialization in power conversion. He is currently an Assistant Professor, Eaton Faculty Fellow, Associate Director of the Energy GRID Institute, and Associate Director of the electric power engineering program with the Department of Electrical and Computer Engineering at the University of Pittsburgh, Swanson School of Engineering. His research interests include electric power conversion, medium to high voltage power electronics, general power electronic converter design (topology, controller design, magnetics), resonant converters and high power density design, power semiconductor evaluation (SiC and GaN) and reliability assessment, aerospace power conversion systems, electric vehicle motor drives, solid state transformers, and power electronics in microgrid applications.

Dr. Grainger is a member of the IEEE Power Electronics Society (PELS) and Industrial Electronics Society (IES) and is an Annual Reviewer of various power electronic conferences and transaction articles. Dr. Grainger served as the IEEE Pittsburgh PELS Chapter Chair for the three years for which the section has won numerous awards under his leadership. In his career thus far, he has contributed to 70+ articles in the general area of electric power engineering (emphasis on electric power conversion) and all of which have been published through the IEEE, *American Society of Naval Engineers*, or *American Society of Engineering Education*.